

EVOLUTION OF NUCLEAR STAR CLUSTERS

DAVID MERRITT

Department of Physics, 85 Lomb Memorial Drive, Rochester Institute of Technology, Rochester, NY 14623

and

Center for Computational Relativity and Gravitation, School of Mathematical Sciences, 78 Lomb Memorial Drive, Rochester Institute of Technology, Rochester, NY 14623

Draft version October 24, 2018

Abstract

Two-body relaxation times of nuclear star clusters are short enough that gravitational encounters should substantially affect their structure in 10 Gyr or less. In nuclear star clusters without massive black holes, dynamical evolution is a competition between core collapse, which causes densities to increase, and heat input from the surrounding galaxy, which causes densities to decrease. The maximum extent of a nucleus that can resist expansion is derived numerically for a wide range of initial conditions; observed nuclei are shown to be compact enough to resist expansion, although there may have been an earlier generation of low-density nuclei that were dissolved. An evolutionary model for NGC 205 is presented which suggests that the nucleus of this galaxy has already undergone core collapse. Adding a massive black hole to a nucleus inhibits core collapse, and nuclear star clusters with black holes always expand, due primarily to heat input from the galaxy and secondarily to heating from stellar disruptions. The expansion rate is smaller for larger black holes due to the smaller temperature difference between galaxy and nucleus when the black hole is large. The rate of stellar tidal disruptions and its variation with time are computed for a variety of initial models. The disruption rate generally decreases with time due to the evolving nuclear density, particularly in the faintest galaxies, assuming that scaling relations derived for luminous galaxies can be extended to low luminosities.

Subject headings: galaxies: evolution – galaxies: nuclei – galaxies: dynamics

1. INTRODUCTION

Many galaxies have compact stellar nuclei. A nearby example is NGC 205, the dwarf elliptical (dE) companion to the Andromeda galaxy. NGC 205 exhibits a sharp upturn in its surface brightness profile inside of a few arcseconds, attributable at least in part to a population of young stars near the center (Hodge 1973; Carter & Sadler 1990). The mass of the nucleus is $\sim 10^6 M_\odot$ and its radius is ~ 10 pc (Jones et al. 1996; Valluri et al. 2005). Reaves (1977) and Romanishin et al. (1977) found similar central light excesses in many early-type galaxies in the Virgo cluster; Binggeli et al. (1987), in their comprehensive survey of Virgo, found that roughly one-fourth of the dwarf (dE and dS0 type) galaxies were nucleated. The nuclei in the Virgo galaxies are sufficiently compact that they appear unresolved in ground-based images, and their detection in these photographic surveys was facilitated by the low central surface brightnesses of dwarf galaxies.

Recent observations with the Hubble Space Telescope have revealed that nuclear star clusters are present in a much wider variety of galaxies, including luminous elliptical galaxies and the bulges of spiral galaxies (Carollo et al. 1997, 1998; Böker et al. 2002; Côté et al. 2006). The fraction of galaxies with clearly distinguishable nuclear clusters is now believed to be as high as 50%-75%. The nuclei are not present in E galaxies brighter than absolute blue magnitude $M_B \approx -19$, but this may be due to the steeply-rising luminosity profiles in these galaxies which would make detection of a nuclear excess difficult. The frequency of nucleation also appears to drop in the faintest galaxies, falling essentially to zero at galaxy absolute magnitudes $M_B \approx -12$ and below (Sandage et al. 1985; van den Bergh 1986).

Nuclear star clusters have the following properties (Böker 2007; van der Marel et al. 2007, and references therein). (a)

They are 10-100 times brighter than typical Milky Way globular clusters. (b) Their sizes correlate with their luminosities as $r \sim L^{0.5}$. (c) Spectra reveal extended star formation histories, and the luminosity-weighted mean stellar age correlates with galaxy Hubble type, from ~ 10 Myr in late-type spirals to ~ 10 Gyr in ellipticals. However the mass is typically dominated by an old stellar population. (d) Nuclear masses correlate with host galaxy (bulge) masses as $M_{\text{nuc}} \approx 0.003 M_{\text{bulge}}$, as well as with other global properties of the bulge such as velocity dispersion and Sérsic index.

The fact that nuclear star clusters obey similar scaling relations with host galaxy properties as do supermassive black holes has led to the suggestion that there may be a fundamental connection between the two classes of object (Ferrarese et al. 2006a; Wehner & Harris 2006): perhaps both should be assigned to the single category of “central massive object”. This suggestion raises the question of whether nuclear star clusters can co-exist with supermassive black holes. Seth et al. (2008) list roughly a dozen galaxies with nuclear emission lines or X-ray luminosities indicative of an active nucleus, and which also contain nuclear star clusters.

This paper addresses the evolution of nuclear star clusters due to random gravitational encounters between stars. Ignoring the possible presence of a massive black hole, relaxation times in the nuclei work out to be about an order of magnitude longer than those in globular clusters, but still short enough that gravitational encounters would substantially affect their structure after 10 Gyr. For instance, in NGC 205, which has one of the best-resolved nuclear star clusters, the central relaxation time is only $\sim 10^8$ yr, short enough that core collapse could have already occurred (Jones et al. 1996; Valluri et al. 2005).

As pointed out by Dokuchaev & Ozernoi (1985), Kandrup (1990) and Quinlan (1996), evolution of a star cluster at the

center of a galaxy can be qualitatively different than that of an isolated stellar system. If the nucleus is sufficiently diffuse, its velocity dispersion will be lower than that of the surrounding galaxy, and the usual tendency toward core collapse will be opposed by a flow of energy from galaxy to nucleus. The fate of the nucleus – collapse versus expansion – depends on whether the core collapse time is short or long compared to the time for the nucleus to absorb energy from the galaxy. Quinlan (1996) analyzed a simple family of two-component models and derived a condition for the minimum compactness of a nucleus in order to resist expansion. Quinlan’s condition implies a maximum size $r_{\text{nuc}}/r_{\text{gal}} \approx 0.02$ for nuclei with masses $M_{\text{nuc}}/M_{\text{gal}} = 10^{-3}$. This is intriguingly close to the observed sizes of nuclear star clusters.

Even a nucleus compact enough to satisfy Quinlan’s criterion could escape core collapse if it contained a black hole. A black hole also acts as a heat source, by destroying and absorbing stars (Shapiro 1977). Nuclear star clusters containing massive black holes should therefore expand, regardless of their initial degree of compactness.

In this paper, integrations of the orbit-averaged Fokker-Planck equation are carried out for models of nucleated galaxies with and without black holes. The Fokker-Planck model includes a loss term describing scattering of stars into the tidal disruption sphere of a black hole, if present. Physical collisions between stars are ignored, and the mass liberated from disrupted stars is assumed to escape instantaneously from the galaxy; these are both approximations but not unreasonable ones (e.g. in NGC 205 the timescale for physical collisions is ~ 3 orders of magnitude longer than the relaxation time). Initial conditions are derived from mass models that mimic the observed luminosity profiles of nucleated galaxies. Quinlan’s criterion for black-hole-free nuclei is refined; we find that observed nuclei are either in the core-collapse regime, or have sufficiently long relaxation times that they would not have evolved appreciably in 10 Gyr. In models containing black holes, the dominant process driving nuclear evolution is almost always found to be heating by the galaxy.

The models presented here are idealizations in one important respect: only a single stellar mass group is considered and stellar masses are assumed to be fixed in time. The effects of mass segregation, star formation and stellar evolution are therefore ignored. Multi-mass models will be considered in a later paper. While the calculations presented here have some relevance to nuclear star clusters in all galaxies, the focus is on models that are structurally similar to low-luminosity elliptical galaxies.

Section II summarizes the properties of nuclear star clusters and their host galaxies that are relevant to this study. Sections III and IV describe the results of evolutionary calculations without, and with, black holes, respectively. Section V sums up.

2. NUCLEAR STAR CLUSTERS AND THEIR HOST GALAXIES

2.1. Nucleated Galaxies in the Virgo Cluster

Figure 1a shows half-light radii r_{eff} and masses M_{nuc} of nuclei observed in the ACS Virgo Cluster Survey (Côté et al. 2004). Dashed lines indicate constant values of the half-mass relaxation time

$$t_{rh} = \frac{1.7 \times 10^5 [r_h(\text{pc})]^{3/2} N^{1/2}}{[m/M_\odot]^{1/2}} \text{ years} \quad (1)$$

(Spitzer 1987), with r_h set equal to r_{eff} . The mean stellar mass m was set to one solar mass and N was computed from $N = M_{\text{nuc}}/m$. Half-mass relaxation times for many of the nuclei are less than 10 Gyr.

Figure 1b shows the dependence of relaxation time on galaxy absolute blue magnitude M_B . Relaxation times are plotted both for the nuclei, and for their host galaxies; in the case of the galaxies, r_h in equation (1) was equated with the observed effective radius R_e (e.g. Ciotti 1991) and N was set to M_{gal}/m . Dotted lines are least-squares fits to $\log t_{rh}$ vs. M_B for galaxies and nuclei independently; the fitted relations are

$$\log_{10}(t_{\text{gal}}/\text{yr}) = 14.2 - 0.336(M_B + 16), \quad (2)$$

$$\log_{10}(t_{\text{nuc}}/\text{yr}) = 9.38 - 0.434(M_B + 16) \quad (3)$$

where we have written t_{gal} and t_{nuc} for the half-mass relaxation time of the galaxy and the nucleus respectively. The second of these relations predicts nuclear relaxation times below 0.1 Gyr in galaxies with $M_B \approx -12$, the least luminous galaxies that contain compact nuclei (van den Bergh 1986).

Figure 1c plots nuclei in the size ratio vs mass ratio plane. The symbol sizes in this plot are proportional to $\log_{10} t_{\text{nuc}}$; filled symbols have $t_{\text{nuc}} < 3$ Gyr and open symbols have $t_{\text{nuc}} > 3$ Gyr. There is evidence in this figure for two populations: compact nuclei with short relaxation times and more extended nuclei with long relaxation times. Figure 1a, combined with the knowledge that nuclear masses correlate with galaxy masses (Wehner & Harris 2006; Ferrarese et al. 2006a), implies that the large- t_{nuc} population in Figure 1c is associated with the brightest galaxies. The lack of nuclei with $r_{\text{eff}}/R_e \lesssim 10^{-3}$ probably reflects an observational limitation: at the distance of Virgo, the ACS/WFC pixel scale of ~ 0.049 arc second corresponds to ~ 3.9 pc, or ~ 0.004 times a typical galaxy effective radius of ~ 1 kpc.

2.2. NGC 205

Nuclear star clusters beyond the Local Group are too distant for their structure to be well resolved. The nearby (~ 824 kpc; McConnachie et al. 2005) dE galaxy NGC 205 contains one of the best resolved nuclei. Figure 2 shows surface brightness data of NGC 205 in the *I* band, obtained by combining *HST* ACS observations from Valluri et al. (2005) with ground-based data of Kim & Lee (1998) and Lee (1996). The horizontal axis is $r_{\text{SMA}} [1 - \epsilon(r)]^{1/2}$ where r_{SMA} is the isophotal semi-major axis and ϵ is the ellipticity; NGC 205 is moderately elongated, $\langle \epsilon \rangle \approx 0.5$.

These circularly-symmetrized data were fit to a two-component spherical model defined, in terms of the (3d) luminosity density $j(r)$, as

$$j(r) = j_1(r) + j_2(r) \quad (4)$$

$$j_1(r) = j_{\text{gal}} e^{-b[(r/r_{1/2})^{1/n} - 1]} \quad (5)$$

$$j_2(r) = j_{\text{nuc}} (1 + r^2/r_c^2)^{-\gamma/2}. \quad (6)$$

The galaxy is represented by Einasto’s (1965) law, identical in functional form to the law of Sérsic (1963) that is more typically applied to surface density profiles. The quantity $b(n)$ is chosen such that $r_{1/2}$ is the (3d) radius containing 1/2 of the total mass corresponding to j_1 ; n is an index that controls the curvature of the profile (not to be confused with the Sérsic index; the latter is typically smaller by $\sim 1 - 2$ than the Einasto n that describes the space density). The nucleus is represented by a generalized “Hubble” law; r_c is the core radius

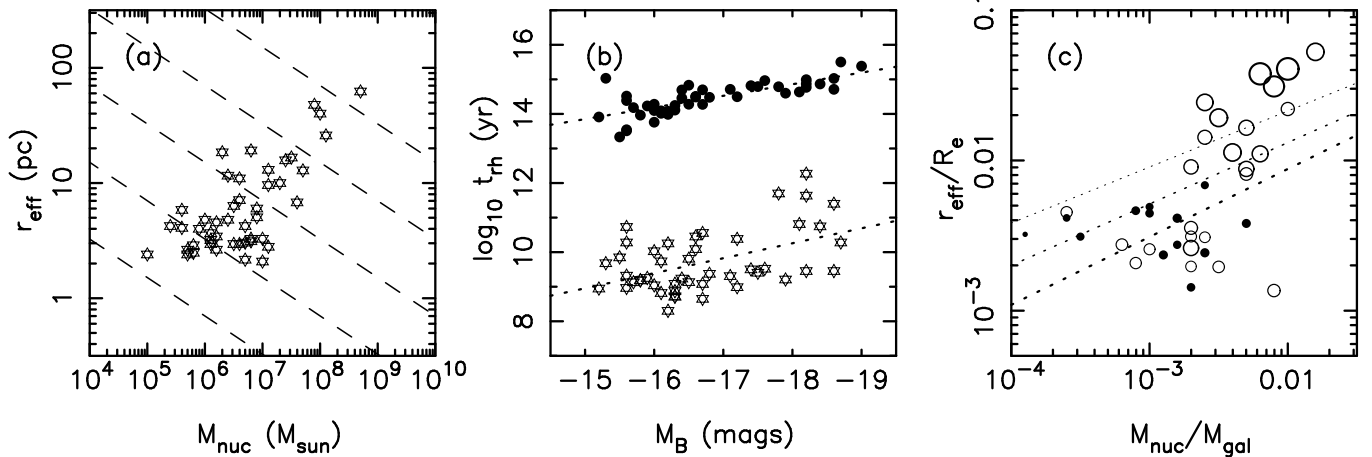


FIG. 1.— Properties of nuclear star clusters in the subset of Virgo cluster early-type galaxies that were found to be nucleated in the ACS Virgo Cluster Survey (Côté et al. 2004). (a) Nuclear radii and masses; masses are from the compilation of Seth et al. (2008). Dashed lines correspond to nuclear half-mass relaxation times of ($10^8, 10^9, 10^{10}, 10^{11}, 10^{12}$) years increasing up and to the right. (b) Half-mass relaxation times of nuclei (stars) and their host galaxies (filled circles). Dotted lines are least-squares fits. (c) Vertical axis is the ratio of half-light radii of nuclei (r_{eff}) to half-light radii of galaxies (R_e); horizontal axis is the ratio of nuclear mass to galaxy mass. Symbol size is proportional to the logarithm of the nuclear relaxation time in (b). Open circles have $\log_{10}(t_{rh}/\text{yr}) \geq 9.5$ and filled circles have $\log_{10}(t_{rh}/\text{yr}) < 9.5$. Dashed lines indicate the critical value of r_{eff}/R_e above which nuclei expand, for galaxies described by Einasto indices $n = 2$ (top), $n = 3$ and $n = 4$ (bottom).

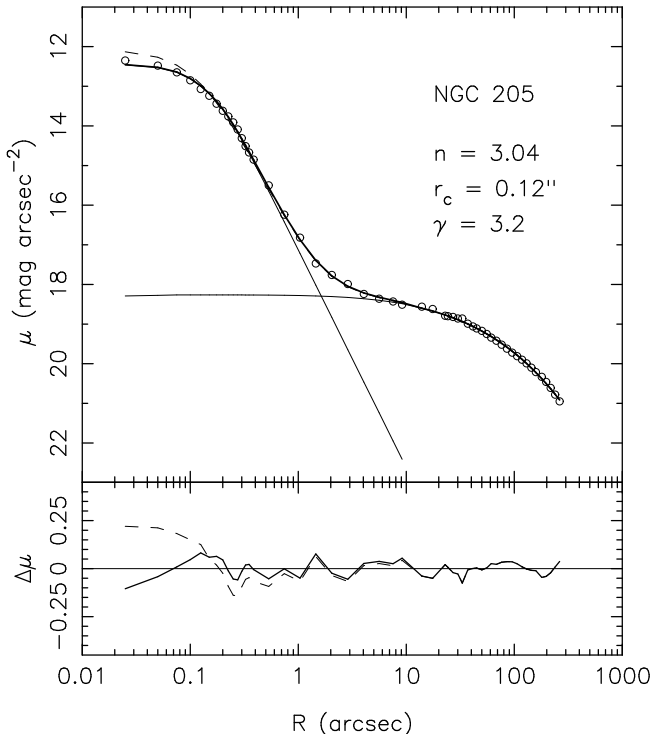


FIG. 2.— Two-component (eq. 2.2) fit to surface brightness data of NGC205. Thin solid lines show the nuclear and galactic components separately, after convolution with the ACS point-spread function; dashed line is before PSF convolution. Lower panel show surface-brightness residuals. n : Einasto index of the galaxy component; r_c : nuclear core radius; γ : power-law index of the nuclear space density.

and γ controls the steepness of the nuclear density falloff, e.g. $\gamma = 5$ is Plummer’s (1911) model and $\gamma = 2$ is the isothermal sphere. Equation (2.2) was compared to the data of Figure 2 after spatial projection and convolution with the circularly-symmetrized ACS HRC point-spread function. The optimization routine adjusted the five parameters ($j_{\text{gal}}, j_{\text{nuc}}, r_{1/2}, r_c, n$) at fixed γ ; the latter parameter was varied in steps of 0.1.

Figure 2 shows the fit that minimizes the surface-brightness

residuals, with $\gamma = 3.2$. The fit is good (~ 0.05 magnitude rms deviation), although this decomposition of the brightness profile into “galaxy” and “nucleus” is not certainly not unique.

Since it provides such a good description of NGC 205, the two-component model of equation (2.2) will be used as a basis for the evolutionary studies described below. We note that one parameter in this fit, the Einasto index n (or rather, the corresponding Sersic index describing the surface brightness profile; Einasto fits have not yet been carried out for many galaxies) is known to correlate roughly with galaxy luminosity, in the sense that brighter galaxies have larger n (Graham & Guzmán 2003).

3. NUCLEAR EVOLUTION WITHOUT BLACK HOLES

We first consider evolution, due to gravitational encounters, of a galaxy containing a compact nucleus consisting of stars with a single mass and no nuclear black hole. Physical collisions between stars are ignored. In this idealized model, evolution takes place on a time scale determined roughly by the central (nuclear) relaxation time, t_{rc} ; stars are scattered into less-bound orbits, transferring heat to the nuclear envelope and causing the central density to increase. If the nucleus were isolated, and ignoring sources of heat like hard binary stars, core collapse would take place in a time of $\sim 10^2 t_{rc}$ (Spitzer 1987). However because the nucleus is embedded in a galaxy, flow of heat can also take place in the opposite sense, from galaxy to nucleus, causing the latter to expand; core collapse is then delayed until a much longer time has elapsed (Quinlan 1996).

3.1. Evolution timescales

We begin by deriving an approximate expression for the time scale to transfer energy from a galaxy to a nucleus, then derive an approximate condition for heating to reverse core collapse. Our approach is similar to treatments in Dokuchaev & Ozernoi (1985) and Kandrup (1990).

Consider a two-component system consisting of galaxy and nucleus. Both components are assumed homogeneous and are characterized by a density ($\rho_{\text{gal}}, \rho_{\text{nuc}}$), radius ($r_{\text{gal}}, r_{\text{nuc}}$), rms velocity ($V_{\text{gal}}, V_{\text{nuc}}$), and half-mass relaxation time ($t_{\text{gal}}, t_{\text{nuc}}$).

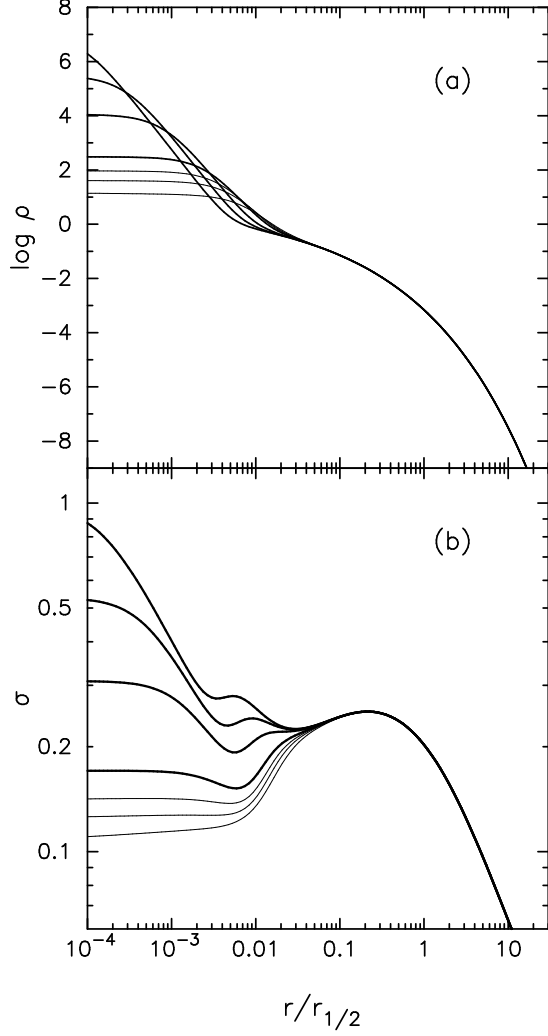


FIG. 3.— Density (upper) and velocity dispersion (lower) profiles of a set of galaxy models constructed according to equation (2.2), normalized such that $G = M_{\text{gal}} = 1$. All models have $M_{\text{nuc}}/M_{\text{gal}} = 0.003$, $n = 3$ and $\gamma = 4$. Different curves correspond to different degrees of nuclear compactness, i.e. $\log_{10}(r_{\text{nuc}}/r_{\text{gal}}) = (-3.72, -3.20, -2.72, -2.20, -2.02, -1.90, -1.72)$. Thick lines denote models in which the nucleus undergoes “prompt” core collapse; thin lines are models in which heat transfer from the galaxy causes the nucleus to expand initially (as show in Fig. 4).

Define $\epsilon_{\text{nuc}} \equiv (1/2)\rho_{\text{nuc}}V_{\text{nuc}}^2$ to be the kinetic energy per unit volume of the nucleus. Assuming Maxwellian velocity distributions and a single stellar mass m , the rate of change of ϵ_{nuc} due to gravitational encounters is

$$\frac{d\epsilon_{\text{nuc}}}{dt} = 4\sqrt{6}\pi G^2 m \rho_{\text{nuc}} \rho_{\text{gal}} \ln \Lambda \frac{(V_{\text{gal}}^2 - V_{\text{nuc}}^2)}{(V_{\text{gal}}^2 + V_{\text{nuc}}^2)^{3/2}} \quad (7)$$

(Spitzer 1987, eq. 2-60). A necessary and sufficient condition for the nucleus to be heated by the galaxy is $V_{\text{gal}} > V_{\text{nuc}}$. When this condition is satisfied, the nuclear heating time is

$$\tau_{\text{heat}} \equiv \left| \frac{1}{\epsilon_{\text{nuc}}} \frac{d\epsilon_{\text{nuc}}}{dt} \right|^{-1} \quad (8)$$

$$= \frac{1}{48} \sqrt{\frac{6}{\pi}} \frac{V_{\text{nuc}}^3}{G^2 m \rho_{\text{nuc}} \ln \Lambda} \left(\frac{\rho_{\text{nuc}}}{\rho_{\text{gal}}} \right) \frac{(V_{\text{gal}}^2/V_{\text{nuc}}^2 + 1)^{3/2}}{(V_{\text{gal}}^2/V_{\text{nuc}}^2 - 1)} \quad (9)$$

In the limiting case $V_{\text{gal}} \gg V_{\text{nuc}}$ this becomes

$$\tau_{\text{heat}} = \left(\frac{\rho_{\text{nuc}}}{\rho_{\text{gal}}} \right) \left(\frac{V_{\text{gal}}}{V_{\text{nuc}}} \right) \frac{1}{48} \sqrt{\frac{6}{\pi}} \frac{V_{\text{nuc}}^3}{G^2 m \rho_{\text{nuc}} \ln \Lambda} \quad (10)$$

$$\approx \left(\frac{\rho_{\text{nuc}}}{\rho_{\text{gal}}} \right) \left(\frac{V_{\text{gal}}}{V_{\text{nuc}}} \right) t_{\text{nuc}} \approx \left(\frac{V_{\text{gal}}}{V_{\text{nuc}}} \right)^2 t_{\text{gal}} \quad (11)$$

$$\approx \left(\frac{\rho_{\text{nuc}}}{\rho_{\text{gal}}} \right)^{1/2} \left(\frac{V_{\text{nuc}}}{V_{\text{gal}}} \right)^{1/2} (t_{\text{nuc}} t_{\text{gal}})^{1/2}. \quad (12)$$

Models that satisfy the condition $V_{\text{gal}} > V_{\text{nuc}}$ have $\rho_{\text{nuc}} \gtrsim \rho_{\text{gal}}$. Thus, the nuclear heating time is of the same order as, or somewhat less than, the geometric mean of t_{nuc} and t_{gal} . According to Figure 1b, this time is shorter than 10 Gyr in at least some galaxies.

Heating from the galaxy will reverse core collapse if τ_{heat} is shorter than the nuclear core collapse time. One definition of the latter time is

$$\tau_{\text{cc}} \equiv \left| \frac{1}{\rho_{\text{nuc}}} \frac{d\rho_{\text{nuc}}}{dt} \right|^{-1} = \xi^{-1} t_{\text{nuc}} \quad (13)$$

where ξ^{-1} varies from ~ 10 in the early stages of core collapse to an asymptotic value of ~ 300 (e.g. Cohn 1980). The condition $\tau_{\text{heat}} < \tau_{\text{cc}}$ becomes

$$\frac{\rho_{\text{nuc}} V_{\text{gal}}}{\rho_{\text{gal}} V_{\text{nuc}}} < \xi^{-1} \quad (14)$$

where $V_{\text{gal}} \gg V_{\text{nuc}}$ has again been assumed. This expression is similar to equation (14) of Dokuchaev & Ozernoi (1985). We can convert equation (14) into a relation between the quantities plotted in Figure 1 by writing $\rho_{\text{nuc}} \approx M_{\text{nuc}}/r_{\text{nuc}}^3$ and by applying the virial theorem separately to both components, i.e.

$$V_{\text{nuc}}^2 \sim \frac{GM_{\text{nuc}}}{r_{\text{nuc}}}, \quad V_{\text{gal}}^2 \sim \frac{GM_{\text{gal}}}{r_{\text{gal}}}; \quad (15)$$

the former expression will only be approximately true for low-density nuclei. With these substitutions, the condition (14) becomes

$$\frac{M_{\text{nuc}}}{M_{\text{gal}}} \lesssim 10^4 \left(\frac{\xi^{-1}}{100} \right)^2 \left(\frac{r_{\text{nuc}}}{r_{\text{gal}}} \right)^5. \quad (16)$$

Setting $M_{\text{nuc}}/M_{\text{gal}} = 0.003$, equation (16) implies that $r_{\text{nuc}}/r_{\text{gal}}$ must be smaller than ~ 0.05 in order for core collapse to occur, a value that lies within the range of observed nuclear sizes (Fig. 1c). While the numerical coefficients in equation (16) should not be considered accurate, the general form of the relation will be verified below via more realistic evolutionary models.

3.2. Fokker-Planck model

Evolution was modelled using the isotropic, orbit-averaged Fokker-Planck equation (Cohn 1980), in the implementation described by Merritt et al. (2007). The initial galaxy was given a density law as defined by equation (2.2); the self-consistent gravitational potential and isotropic phase-space distribution functions were derived from Poisson’s and Edington’s formulae respectively. Henceforth we characterize these initial models by the two dimensionless parameters

$$r_{\text{nuc}}/r_{\text{gal}}, \quad M_{\text{nuc}}/M_{\text{gal}} \quad (17)$$

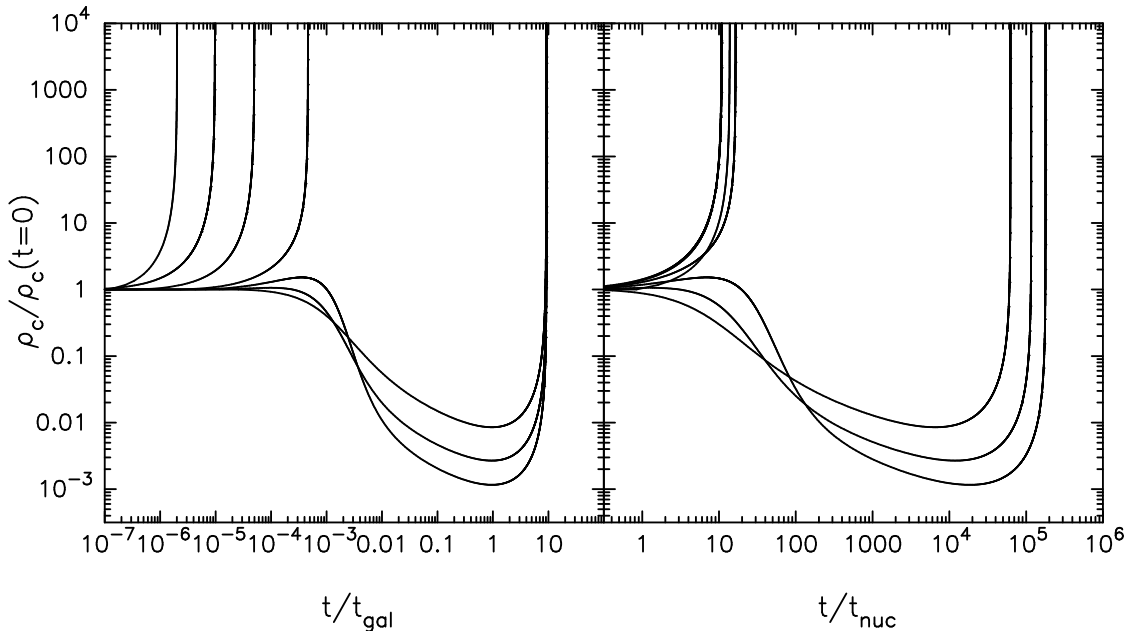


FIG. 4.— Evolution toward core collapse in the galaxy models plotted in Fig. 3. Vertical axis is the core density normalized to its initial value. The horizontal axis is the time in units of the initial, half-mass relaxation time t_{rh} , defined by the galaxy (left) or by the nucleus (right).

where r_{nuc} and r_{gal} are the spatial (not projected) half-mass radii of nucleus and galaxy respectively, and M_{nuc} and M_{gal} are the total masses corresponding to the two components. Given the varied and non-unique ways in which half-light radii are defined observationally, we will henceforth simply identify r_{nuc}/r_{gal} with r_{eff}/R_e when comparing models to data. (This identification should probably only be trusted to within a factor of two or so.)

Figure 3 shows $\rho(r)$ and $\sigma(r)$ for a set of galaxy models with Einasto index $n = 3$ and nuclear slope $\gamma = 4$; $\sigma(r)$ is the 1d velocity dispersion. Each of these models has $M_{nuc}/M_{gal} = 0.003$ but they differ in their degree of nuclear concentration, from $r_{nuc}/r_{gal} \approx 0.0002$ to ~ 0.03 . The dependence of σ on r is complex, sometimes exhibiting multiple maxima; but as the nucleus is made less compact, the central velocity dispersion drops, and when $r_{nuc}/r_{gal} \gtrsim 0.003$ the central σ is lower than the peak value in the outer galaxy. “Temperature inversions” like these imply a flow of heat from galaxy to nucleus, which tends to counteract the outward flow that would otherwise drive the nucleus toward core collapse (Dokuchaev & Ozernoi 1985).

Figure 4 shows the change with time of the central densities of the models in Figure 3. Times are normalized by the initial, half-mass relaxation time; the left panel normalizes to the galactic relaxation time t_{gal} , and the right panel to t_{nuc} . There is a critical value of r_{nuc}/r_{gal} above which evolution toward core collapse is halted and the nucleus expands. Core collapse still occurs in these models but on a much longer time scale, roughly ten times the galaxy half-mass relaxation time (and far longer than galaxy lifetimes; see Fig. 1b). The delay is due, as first shown by Quinlan (1996), to the galaxy’s need to first reverse the temperature gradient near the center by creating a large, flat core. In the models with nuclei that contract, core collapse occurs in 15–20 times the initial nuclear half-mass relaxation time.

Experiments like the ones illustrated in Fig. 4 were carried out for initial models with a range of r_{nuc}/r_{gal} and M_{nuc}/M_{gal} values, and with Einasto indices $n = (3, 4, 5)$. The critical

size ratio that separates collapsing-core and expanding-core models is plotted in Figure 1c for the three different values of n . The critical values are well fit by relations of the form

$$\frac{M_{nuc}}{M_{gal}} = A \left(\frac{r_{nuc}}{r_{gal}} \right)^B \quad (18)$$

where

$$\begin{aligned} n = 2 : A = 300, B = 2.70 \\ n = 3 : A = 390, B = 2.45 \\ n = 4 : A = 355, B = 2.20. \end{aligned} \quad (19)$$

Quinlan (1996) derived a similar criterion for double-Plummer-law galaxy models; his relation is most similar to the one found here for $n = 2$, which is reasonable given the low central concentration of Plummer models. While these results are all based on nuclei with $\rho \sim r^{-4}$ envelopes, we note that half-mass radii are nearly invariant to the structural changes that occur prior to core collapse. Hence the criteria of equation (19) should apply approximately to a much broader class of models, including models in which the nucleus evolved toward core collapse starting from the initial conditions adopted here.

Interestingly, Figure 1c shows that observed nuclei almost all lie in the “prompt” core collapse regime; the only clear exceptions are nuclei with such long relaxation times ($\gtrsim 10$ Gyr) that very little evolution would have occurred since their formation.

It would be nice to go one step further and argue that the paucity of nuclei above the critical lines in Figure 1c is due to dynamical evolution, i.e. that there once existed a population of low-density nuclei that underwent expansion and that now have such low densities that they are no longer observable as distinct components. This argument is valid only if dissolution time scales for the nuclei in this region of the plot are shorter than ~ 10 Gyr. This is true for some, but not all, possible initial conditions. In models near but above the critical line, the time for the central density to drop by a factor ~ 2 is

found to be $\sim 10^{-4} t_{\text{gal}}$ for $M_{\text{nuc}}/M_{\text{gal}} \lesssim 3 \times 10^{-4}$ but increases to $\sim 10^{-3} t_{\text{gal}}$ for the more typical value $M_{\text{nuc}}/M_{\text{gal}} \lesssim 3 \times 10^{-4}$ (e.g. Fig. 4). The latter time is longer than 10 Gyr in almost all galaxies.

Finally, we consider the special case of NGC 205 (Fig. 2). On which side of the divide does it lie? Dynamical modelling of NGC 205 suggests that the nuclear mass-to-light ratio is \sim a few times smaller than that of the galaxy as a whole (Carter & Sadler 1990; Valluri et al. 2005). To construct a mass model, we therefore simply decreased the amplitude of the nuclear component in the luminosity profile fit of Figure 2 by a factor of 0.3 at all radii. Figure 5 shows the projected “surface brightness” of this mass model, i.e., $-2.5 \log \Sigma$, where $\Sigma(R)$ is the mass surface density at projected radius R . The $r_{\text{nuc}}/r_{\text{gal}}$ and $M_{\text{nuc}}/M_{\text{gal}}$ values for this mass model place NGC 205 close enough to the critical lines in Figure 1c that its fate is difficult to judge.

Accordingly, a variety of initial models (all with $n = 3.04$ and $\gamma = 4$) were constructed and integrated forward for ~ 10 Gyr to see if any could match the reconstructed mass profile of NGC 205. Figure 5 shows the results of one such exercise: this initial model undergoes “prompt” core collapse, achieving singular density in a time of $\sim 1.0 \times 10^{-4}$ galaxy half-mass relaxation times, i.e. $\sim 10^{10}$ yr. The final, projected mass profile is essentially identical to that of NGC 205 except at $R \lesssim 0.1''$ where the data suggest a flat core; this difference is probably not significant however given that the luminosity profile is not well constrained at radii smaller than the PSF. (Alternatively, NGC 205 might not have reached full core collapse; or some process like binary heating might have caused the core to re-expand.) While not conclusive, this and similar experiments suggest that the luminosity profile of NGC 205 is consistent with this galaxy’s nucleus having undergone core collapse at some time in the last 10 Gyr.

It is interesting to note that even slight reductions in the central density of the initial model in Figure 5 (larger r_{nuc} , smaller M_{nuc}) led to expansion rather than collapse. In other words: if its formation history had been only slightly different, NGC 205 might no longer contain a compact nucleus.

4. NUCLEAR EVOLUTION WITH BLACK HOLES

4.1. Models and Assumptions

Next we consider the evolution of nucleated galaxies containing massive black holes; the latter are idealized as Newtonian point masses with fixed mass M_{bh} . Evolution of $f(E)$ describing the stars is again followed via the orbit-averaged Fokker-Planck equation with evolving potential, including the (fixed) potential from the black hole, and with a modification that accounts for the loss of stars that are scattered into the black hole’s sphere of tidal disruption (Merritt et al. 2007). The latter is assigned a radius of r_t where

$$r_t = \left(\eta^2 \frac{M_{\text{bh}}}{m} \right)^{1/3} r_* \quad (20)$$

with r_* a stellar radius and $\eta \approx 0.844$, the value appropriate to an $n = 3$ polytrope. If $E = -v^2/s + \psi(r)$ is the binding energy per unit mass of a star in the combined potential of the galaxy and black hole, then the tidal disruption sphere defines a “loss cone” of orbits with angular momenta J such that $J \lesssim J_{\text{lc}}(E)$, where

$$J_{\text{lc}}^2(E) = 2r_t^2 [\psi(r_t) - E] \approx 2GM_{\text{bh}}r_t. \quad (21)$$

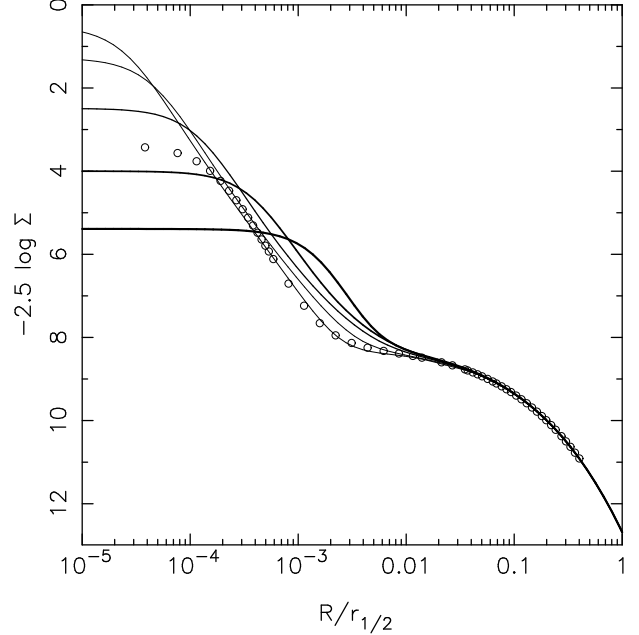


FIG. 5.— Open circles show the surface “mass density” of a model of NGC 205 derived from Fig. 2; the normalization of the nuclear component was reduced by a factor of 0.3 relative to that of the galaxy to account for the lower mass-to-light ratio of the nucleus. Heavy solid line shows a mass model that was integrated forward via the Fokker-Planck equation; progressively thinner lines show the surface density profile at (0.8, 0.98, 0.997, 0.9995) times the core collapse time of ~ 10 Gyr.

For black hole masses of interest here ($M_{\text{bh}} < 10^8 M_{\odot}$), r_t is always greater than the radius of the event horizon, i.e. stars are disrupted not swallowed.

The Fokker-Planck equation now has the form

$$\frac{\partial N}{\partial t} = -\frac{\partial F_E}{\partial E} - \mathcal{F}(E, t). \quad (22)$$

Here, $N(E, t)$ is the distribution of stellar energies; $\mathcal{F}(E, t)$ is the flux of stars per unit of energy that are scattered in the angular-momentum direction into the tidal disruption sphere; and $F_E(E, t)$ is the energy-directed flux. Each of these terms is defined in detail in Merritt et al. (2007).

Three additional, dimensionless parameters are associated with the black hole models: r_t/r_{gal} , $M_{\text{bh}}/M_{\text{gal}}$, and $N \equiv M_{\text{gal}}/m$. The first of these can be written

$$\frac{r_t}{r_{\text{gal}}} = 2.0 \times 10^{-9} \left(\frac{r_{\text{gal}}}{1 \text{ kpc}} \right)^{-1} \left(\frac{M_{\text{bh}}/m}{10^6} \right)^{1/3} \left(\frac{r_*}{R_{\odot}} \right). \quad (23)$$

In the “empty loss cone” limit, the tidal disruption rate varies only logarithmically with r_t (Lightman & Shapiro 1977). The dependence on r_t is steeper if the loss cone is partially full (as is the case in these models); nevertheless, here we simply fix $r_* = R_{\odot}$ and $m = M_{\odot}$. Furthermore, half-light radii for dE galaxies average ~ 1 kpc with a very weak dependence on galaxy luminosity (although with considerable scatter; Graham & Guzmán (2003)) and so we set

$$\frac{r_t}{r_{\text{gal}}} = 4.5 \times 10^{-9} \left(\frac{N}{10^{10}} \right)^{1/3} \left(\frac{10^3 M_{\text{bh}}}{M_{\text{gal}}} \right)^{1/3}. \quad (24)$$

Equation (24) gives the first of the three new parameters in terms of the other two.

We relate N in this expression to observable galaxy properties by setting $m \approx M_{\odot}$ and expressing M_{gal} in terms of galaxy

absolute magnitude. A typical B-band mass-to-light ratio for dE galaxies is $2 \lesssim (M/L)_B \lesssim 4$ in Solar units (e.g. Seth et al. 2008) so the relation between M_B and N is roughly

$$\log_{10} N \approx 10 - 0.4(M_B + 18). \quad (25)$$

In the evolutionary models presented above, N was a trivial parameter, affecting only how the time unit of the calculation (essentially the relaxation time) was converted into years (e.g. eq. 1). In models containing a black hole, N also fixes the ratio between orbital periods $P(E)$ and the (orbit-averaged) time scales for diffusional loss-cone refilling, or

$$q(E) \equiv \frac{1}{R_{lc}(E)} \oint \frac{dr}{v_r} \lim_{R \rightarrow 0} \frac{\langle (\Delta R)^2 \rangle}{2R} \quad (26)$$

$$\approx P(E) R_{lc}(E)^{-1} t_r^{-1}. \quad (27)$$

Here $R \equiv J^2/J_c(E)^2$ is a dimensionless angular momentum variable, $0 \leq R \leq 1$, with $J_c(E)$ the angular momentum of a circular orbit of energy E , and $\langle (\Delta R)^2 \rangle$ is the diffusion coefficient associated with R . For a galaxy with given structural parameters (M_{gal}, r_{gal}), $q \propto N^{-1}$. Small/large q (i.e. large/small N) correspond to empty/full loss cone regimes respectively (Lightman & Shapiro 1977). We adopt the prescription of Cohn & Kulsrud (1978) for relating the loss cone flux \mathcal{F} to the phase-space density f given q . The integrated loss rate, $\int \mathcal{F}(E) dE$, is denoted by \dot{M} . The contributions of the masses of tidally disrupted stars either to the galactic potential or to the mass of the black hole are ignored.

Masses of (putative) black holes in dE galaxies are poorly constrained, and so several values for the last of the three parameters M_{bh}/M_{gal} were tried, in the range $10^{-4} \leq M_{bh}/M_{gal} \leq 0.03$.

In order to accommodate a black hole, a slight modification to the equilibrium galaxy models of equation (2.2) was required. In an isotropic stellar system containing a central point mass, the central density must increase at least as fast as $r^{-1/2}$ in order for $f(E)$ to remain nonnegative. The flat nuclear density profile of equation (2.2) was therefore changed to a $\rho \propto r^{-0.5}$ dependence inside $r \approx r_c$.

In what follows, we fixed the following parameter values:

$$\gamma = 4, \quad n = 3. \quad (28)$$

Setting $n = 3$ is reasonable given the weak observed dependence of galaxy Sersic index on M_B for dE galaxies (Graham & Guzmán 2003), but we note again that our models should not be scaled to giant E galaxies which have steeper central density profiles. We then carried out four series of integrations, starting from initial models with the following parameters:

- Series I: $M_{nuc}/M_{gal} = 3 \times 10^{-3}$, $M_{bh}/M_{gal} = 1 \times 10^{-3}$. The parameter r_{nuc}/r_{gal} was varied from 2×10^{-4} to 3×10^{-2} . The two mass ratios that define this series of models are close to the average observed values (Ferrarese & Ford 2005; Ferrarese et al. 2006a).
- Series II: $r_{nuc}/r_{gal} = 3 \times 10^{-4}$. The nuclear mass was varied over the range $1 \times 10^{-4} \leq M_{nuc}/M_{gal} \leq 3 \times 10^{-2}$ and the black hole mass was set to $M_{nuc}/3$.
- Series III: $M_{nuc}/M_{gal} = 3 \times 10^{-3}$, $r_{nuc}/r_{gal} = 3 \times 10^{-4}$. The black hole mass was varied over the range $10^{-4} \leq M_{bh}/M_{gal} \leq 3 \times 10^{-2}$.

The number of stars in Series I-III was fixed at $N = 10^{10}$, appropriate for a $M_B \approx -18$ galaxy (eq. 25). As discussed below, the choice of N has very little effect on the evolution of the density profile, and the results for $\rho(r, t)$ can robustly be scaled to galaxies of different luminosities after adjusting the value of t_{gal} . The assumed value of N does, however, substantially affect the dynamics of the loss cone and the rate of tidal disruptions, and to investigate this dependence a fourth series of integrations were carried out:

- Series IV: $M_{nuc}/M_{gal} = 3 \times 10^{-3}$, $r_{nuc}/r_{gal} = 1 \times 10^{-3}$, $M_{bh}/M_{gal} = 1 \times 10^{-3}$. The parameter N was varied from 10^6 to 10^{11} ; according to equation (25), this corresponds to a range in galaxy absolute magnitude $-8 \gtrsim M_B \gtrsim -20.5$.

Each integration was continued until a time of roughly $0.1 t_{gal}$. Using equations (25) and (2), this corresponds to $\sim 10^{14}$ yr for $M_B = -18$, 10^{13} yr for $M_B = -15$, 10^{12} yr for $M_B = -12$, and 10^{11} yr for $M_B = -9$.

In a galaxy containing a massive black hole, the nuclear half-mass relaxation time is not a well defined quantity. Instead, we will cite below the local relaxation time $t_r(r)$ in these models, defined as

$$t_r(r) = \frac{0.34 \sigma(r)^3}{\rho(r) m G^2 \ln \Lambda} \quad (29)$$

(Spitzer 1987), where $\sigma(r)$ is the 1d stellar velocity dispersion defined above and includes the contribution to the stellar motions from the presence of the black hole itself. A natural radius at which to evaluate t_r is the black hole's influence radius,

$$r_{bh} = \frac{GM_{bh}}{\sigma_0^2}. \quad (30)$$

In this formula, we set σ_0 equal to its peak value in the black-hole-free model; e.g. for the models of Figure 3 ($n = 3$), $\sigma_0 \approx 0.25$, or

$$r_{bh} = 0.016 \left(\frac{M_{bh}}{0.001} \right) \quad (31)$$

in units where $G = M_{gal} = 1$. This is reasonably equivalent to the way that r_{bh} is defined by observers. Merritt et al. (2007) plot $t_r(r_{bh})$ as a function of σ_0 in a sample of (mostly luminous) galaxies; they find $t_r(r_{bh}) \approx 10^{11} \text{ yr} (\sigma_0/100 \text{ km s}^{-1})^{7.5}$.

As defined here, r_{bh} is essentially time-independent in these simulations, although the values of $\rho(r_{bh})$, $\sigma(r_{bh})$ and hence $t_r(r_{bh})$ do evolve substantially.

4.2. Results: Density Evolution

Models with central black holes evolve differently than models without black holes, in two important ways.

1. On time scales of order the nuclear relaxation time, the density within the black hole's influence sphere attains the $\rho \sim r^{-7/4}$ "zero-flux" Bahcall-Wolf quasi-steady-state form (Bahcall & Wolf 1976, 1977).

2. The presence of the black hole counteracts both the tendency toward core collapse in compact nuclei, and the tendency toward core expansion in low-density nuclei. The black hole's mass – while a small fraction of the total galaxy mass – is always comparable with the mass of the nuclear cluster in

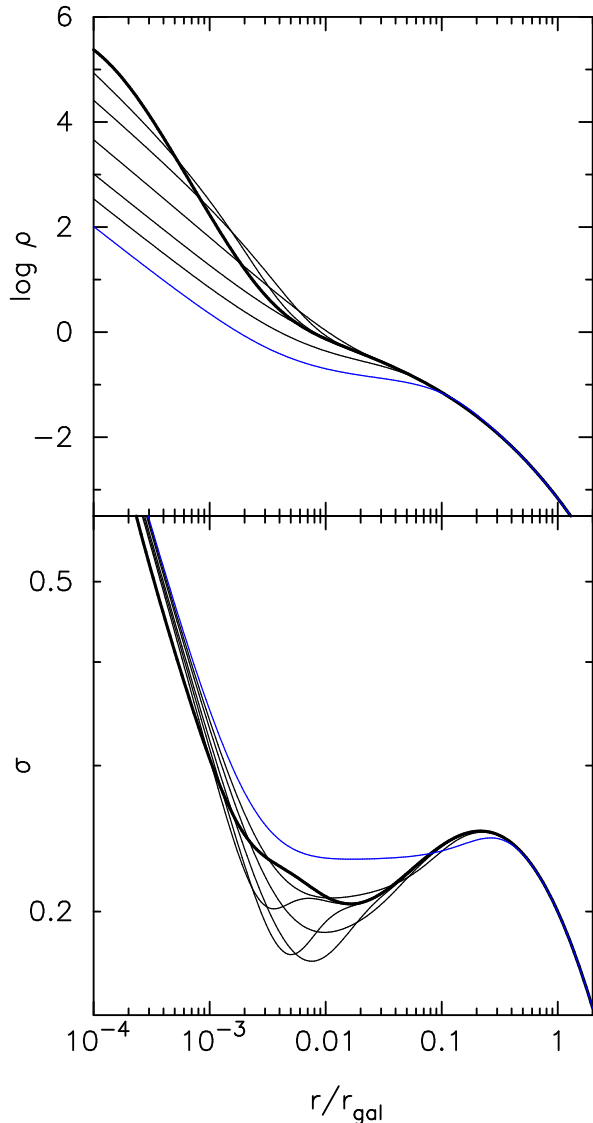


FIG. 6.— Evolution of density (upper) and velocity dispersion (lower) profiles in a model from Series I with $M_{\text{nuc}}/M_{\text{gal}} = 0.003$, $r_{\text{nuc}}/r_{\text{gal}} = 0.0002$ and $M_{\text{bh}}/M_{\text{gal}} = 0.001$. Thick curves are the initial models and blue curves show the final time step; in units of t_{gal} , the displayed times are $(0, 3 \times 10^{-6}, 1 \times 10^{-5}, 1 \times 10^{-4}, 1 \times 10^{-3}, 0.01, 0.1)$.

these models, and the fixed gravitational potential associated with the black hole acts to decouple changes in the central density from changes in the central velocity dispersion, breaking the feedback loop that drives core collapse. Furthermore, in low-density nuclei, the presence of the black hole raises the “temperature” of the nucleus and decreases the inward heat flux from the surrounding galaxy, reducing the expansion rate compared with that of a black-hole-free nucleus.

Because core collapse is suppressed in these models, the long-term evolution ($t \gtrsim t_r(r_{\text{bh}})$) is always toward expansion.

Figure 6 illustrates the evolution of a model from Series I, with $M_{\text{nuc}}/M_{\text{gal}} = 0.003$, $r_{\text{nuc}}/r_{\text{gal}} = 0.0002$ and $M_{\text{bh}}/M_{\text{gal}} = 0.001$. On a time scale of $\sim t_r(r_{\text{bh}}) \approx 10^{-5} t_{\text{gal}}$ the Bahcall-Wolf cusp is established near the black hole and the velocity dispersion drops slightly due to the change in the density slope. At longer times the inward flux of heat from the galaxy begins to erase the dip in the velocity dispersion profile and causes the density to drop.

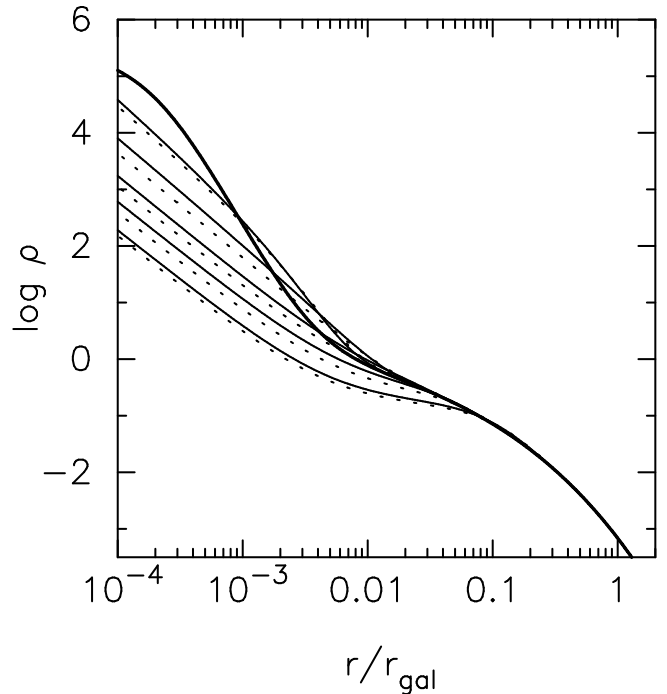


FIG. 7.— Comparison of the density evolution in two integrations including (solid lines) and without (dashed lines) the loss term \mathcal{F} representing tidally disrupted stars. Initial model (heavy line) had $M_{\text{nuc}}/M_{\text{gal}} = 0.003$, $r_{\text{nuc}}/r_{\text{gal}} = 0.0003$ and $M_{\text{bh}}/M_{\text{gal}} = 0.001$. In units of t_{gal} , the displayed times are $(0, 1 \times 10^{-5}, 1 \times 10^{-4}, 1 \times 10^{-3}, 0.01, 0.1)$.

In addition to heat transfer from the galaxy, destruction of stars by the black hole is effectively a heat source which by itself would cause the density of the nucleus to fall (Shapiro 1977). However, integrations in which the loss term $\mathcal{F}(E, t)$ was set to zero evolved almost identically to those which included the loss term. Figure 7 shows an example. Apparently, in all these models, the difference in temperature between nucleus and galaxy, and not the destruction of stars by the black hole, is the dominant effect which causes the nucleus to expand.

Figure 8 illustrates the early evolution of models from Series I-III; the figure shows density profiles at $t = 0$, and after an elapsed time of $10^{-4} t_{\text{gal}}$. The top row of the figure shows the effects of varying the nuclear radius in galaxies with $M_{\text{nuc}}/M_{\text{gal}} = 0.003$ and fixed black hole mass (Series I). In each of these models, the initial velocity dispersion profile exhibits a dip outside $r_{\text{bh}} \approx 0.015$, and the early evolution is a combined result of the inward flow of heat from the galaxy, and formation of the Bahcall-Wolf profile at $r \lesssim r_{\text{bh}}$ due to scattering of stars onto tightly-bound orbits. By $\sim 3 \times 10^{-5} t_{\text{gal}}$ almost all differences between the initial profiles have been erased and the nucleus has been transformed into a $\rho \sim r^{-7/4}$ cusp with a mass approximately equal to the initial nuclear mass.

The middle row of Figure 8 shows the result of varying the nuclear mass at fixed nuclear radius; the black hole mass is set to $M_{\text{nuc}}/3$ (Series II). In low-mass nuclei, the evolution is similar to that of the models in Series I, with the difference that the final normalization of the Bahcall-Wolf cusp is proportional to the initial nuclear mass. For $M_{\text{nuc}} \gtrsim 0.01 M_{\text{gal}}$ ($M_{\text{bh}} \gtrsim 0.003 M_{\text{gal}}$), the initial velocity dispersion profile lacks a local minimum and the heat flow from the galaxy is greatly reduced; the evolution in these models is dominated by for-

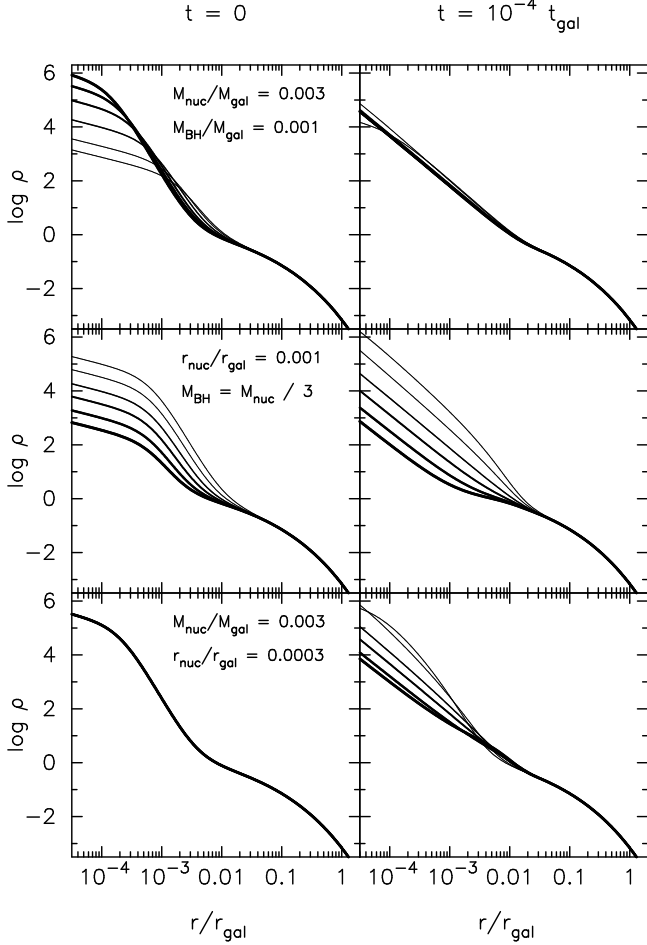


FIG. 8.— Density profiles at $t = 0$ (left) and after an elapsed time of $10^{-4} t_{\text{gal}}$ (right) for various models containing black holes. Line widths correspond between left and right panels. Top: Series I; $r_{\text{nuc}}/r_{\text{gal}} = (2 \times 10^{-4}, 3 \times 10^{-4}, 1 \times 10^{-3}, 3 \times 10^{-3}, 1 \times 10^{-2}, 3 \times 10^{-2})$; line width is a decreasing function of r_{nuc} . Middle: Series II; $M_{\text{nuc}}/M_{\text{gal}} = (1 \times 10^{-4}, 3 \times 10^{-4}, 1 \times 10^{-3}, 3 \times 10^{-3}, 1 \times 10^{-2}, 3 \times 10^{-2})$; line width is a decreasing function of M_{nuc} . Bottom: Series III; $M_{\text{bh}}/M_{\text{gal}} = 1 \times 10^{-4}, 3 \times 10^{-4}, 1 \times 10^{-3}, 3 \times 10^{-3}, 1 \times 10^{-2}, 3 \times 10^{-2}$; line width is a decreasing function of M_{bh} .

mation of the Bahcall-Wolf cusp.

The bottom row of Figure 8 shows the effects of varying the black hole mass on a model with fixed $(M_{\text{nuc}}, r_{\text{nuc}})$ (Series III). Here the differences are due almost entirely to the effect of the black hole on the velocity dispersion profile: larger black holes imply a smaller, initial dip in the temperature profile and less evolution. In these models, the contribution of the loss term to the changes in $\rho(r)$ is most clearly seen, but it is still slight. It is interesting to note that the form of $\rho(r)$ at $r < r_{\text{bh}}$ can depart strongly from the “zero-flux,” $\rho \sim r^{-7/4}$ form at early times in the models with larger black holes.

Evolution of the central density over the full course of the integrations is shown in Figure 9 for the same models in Figure 8. Plotted there is the density at a (fixed) radius of $0.1 r_{\text{bh}}$, normalized to its initial value. Aside from an early increase due to the formation of the $\sim r^{-7/4}$ cusp, the general trend is for the density to decrease; the decrease is smallest (all else equal) for bigger black holes, for the reasons discussed above. For $M_{\text{bh}}/M_{\text{gal}} = 0.001$, the density declines as $\rho \sim t^{-0.5}$ at late times ($t \gtrsim t_{\text{r}}(r_{\text{bh}})$), with steeper(shallower) falloff for smaller(larger) M_{bh} .

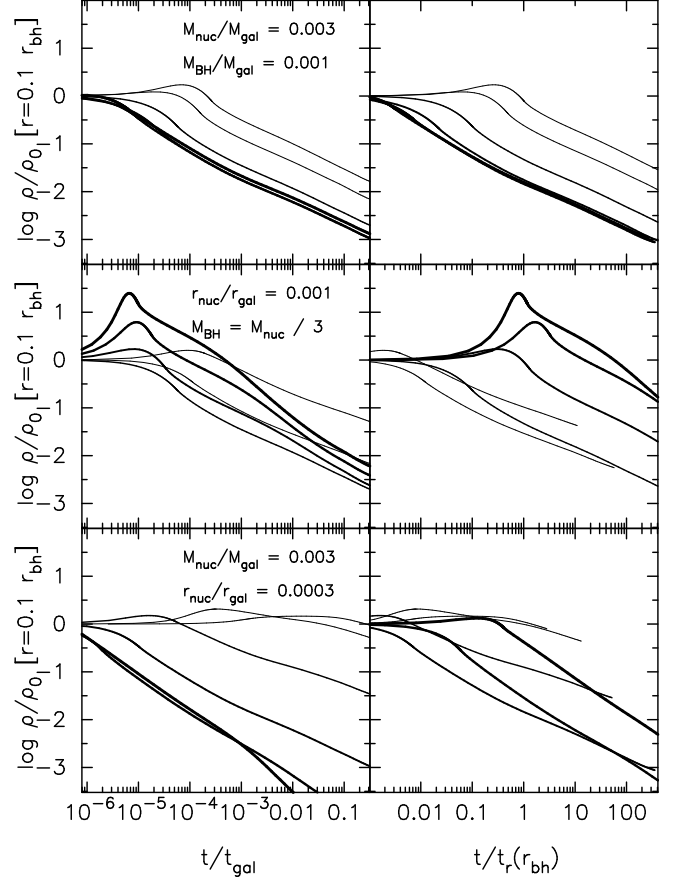


FIG. 9.— Evolution of the central density in the black hole models illustrated in Fig. 8. The vertical axis is the density at a radius of 0.1 times the black hole’s initial influence radius, compared with its value at $t = 0$. Left: time in units of galaxy half-mass relaxation time. Right: time in units of the galaxy’s initial relaxation time evaluated at the black hole’s influence radius.

What do these models imply for the observed properties of nuclear star clusters? The general tendency of the black hole models is to evolve toward lower central density at fixed nuclear size, i.e. to move toward the left on Figure 1, and eventually to disappear from this plot as the nuclei become too diffuse to be detected. Evolution is strongest in the case of models containing nuclei of low initial density and small ($M_{\text{bh}} \lesssim 3 \times 10^{-4} M_{\text{gal}}$) black holes: these galaxies have a strong “temperature inversion,” implying nuclear heating, while the presence of the black hole inhibits core collapse. The heavy curves in the lower left panels of Figures 8 and 9 show that the nuclei in such models are the most rapidly destroyed, and assuming the presence of such “small” black holes in nucleated galaxies would help to explain the lack of points in the upper left part of Figure 1. Larger black holes ($M_{\text{bh}} \gtrsim M_{\text{nuc}}$) tend to stabilize nuclei by reducing the temperature inversion and decreasing the flow of heat from the galaxy. In such models, a Bahcall-Wolf cusp is established in a time $\sim t_{\text{r}}(r_{\text{bh}}) \approx 10^{-5} t_{\text{gal}}$ and little evolution subsequently takes place.

While no attempt was made to construct evolutionary black-hole models that match the current state of NGC 205, it is clear from Figures 8 and 9 that including a black hole of mass $M_{\text{bh}} \gtrsim 10^{-3} M_{\text{gal}}$ in this galaxy would cause the initial configuration to evolve very little over 10 Gyr, aside from the establishment of the $\rho \sim r^{-7/4}$ cusp inside $\sim 0.2 r_{\text{bh}} \approx$

0.1 pc ($M_{\text{bh}}/10^5 M_{\odot}$). The kinematical upper limit to M_{bh} in NGC 205 is $\sim 5 \times 10^4 M_{\odot}$ (Valluri et al. 2005) so the influence of a black hole would be limited to ~ 0.05 pc $\approx 0.02''$, below HST resolution.

4.3. Results: Rates of Stellar Tidal Disruption

An unambiguous signature of a massive black hole is a tidal disruption flare (Komossa & Bade 1999). Figure 10 shows the rate at which mass (in stars) is scattered into the black hole’s disruption sphere for the various models. The left and middle columns of this figure show \dot{M} expressed in units of $M_{\text{gal}}/t_{\text{gal}}$ (which does not change with time) and $M_{\text{bh}}/t_r(r_{\text{bh}})$ respectively; the latter unit is itself a function of time via the time dependence of $\rho(r_{\text{bh}}, t)$ and $\sigma(r_{\text{bh}}, t)$. (We emphasize that the mass of the black hole is assumed constant in these Fokker-Planck models.) The right column in Figure 10 shows the total mass lost to disruptions, integrated from time zero until time t , in units of M_{bh} .

While the variation of mass loss rate with time is complex, the general trend is for \dot{M} to decrease as the nuclear density drops. We consider first a “fiducial” model defined by $M_{\text{nuc}}/M_{\text{gal}} \approx 0.003$ and $M_{\text{bh}}/M_{\text{gal}} \approx 0.001$; these are approximately equal to the average mass ratios that are observed in galaxies with nuclear clusters and black holes respectively (Wehner & Harris 2006; Ferrarese et al. 2006a). We also focus first on the case $N = 10^{10}$ which was assumed in Series I-III; this corresponds to a galaxy absolute magnitude $M_B \approx -18$ (eq. 25) and to $t_{\text{gal}} \approx 7 \times 10^{14}$ yr (eq. 2). By $t = 2 \times 10^{-5} t_{\text{gal}} \approx 15$ Gyr, the Bahcall-Wolf cusp has been established in these models and the loss rate to the black hole is essentially independent of the initial nuclear radius:

$$\dot{M} \approx 0.1 \frac{M_{\text{bh}}}{t_r(r_{\text{bh}})}. \quad (32)$$

\dot{M} remains relatively constant thereafter if expressed in these units. The total mass in disrupted stars at $t \approx 2 \times 10^{-5} t_{\text{gal}}$ in the same subset of models is $\sim 0.02 M_{\text{bh}}$, implying a mean disruption rate over this time of $\sim 10^3 M_{\text{bh}}/t_{\text{gal}}$, or

$$\bar{\dot{M}} \approx 10^{-6} M_{\odot} \text{ yr}^{-1} \left(\frac{M_{\text{bh}}}{10^6 M_{\odot}} \right) \left(\frac{t_{\text{gal}}}{10^{14} \text{ yr}} \right)^{-1}. \quad (33)$$

However, much higher and much lower rates are also possible:

- At early times, before the Bahcall-Wolf cusp is fully established, \dot{M} in the fiducial models is higher for smaller $r_{\text{nuc}}/r_{\text{gal}}$ by as much as \sim an order of magnitude.
- The second row of Figure 10 shows that the initial \dot{M} scales roughly with M_{nuc} for fixed $r_{\text{nuc}}/r_{\text{gal}}$ and $M_{\text{bh}}/M_{\text{nuc}}$.
- The third row of Figure 10 shows that the mass loss rate at early times (i.e. before the nuclear density profile has been strongly affected by the presence of the black hole) is a decreasing function of M_{bh} at fixed $(M_{\text{gal}}, t_{\text{gal}})$, for reasons that were discussed in detail by Wang & Merritt (2004).

The results discussed so far have described the effects on \dot{M} of changing the structural parameters of the initial galaxy. An equally important parameter is the assumed number of stars N . In addition to fixing the unit of time t_{gal} , N also determines the details of the loss-cone refilling process and hence the number of stars scattered into the black hole in one relaxation time. Small N corresponds to a “full loss cone” and large N to an “empty loss cone.” (Small values of M_{bh} also imply

a full loss cone; for instance, in the third row of Fig. 10, the full-loss-cone regime is reached for $M_{\text{bh}}/M_{\text{gal}} \approx 10^{-3}$.)

Recalling the definition of $q(E)$ (eq. 27) as the dimensionless ratio between the orbital period and the loss cone refilling time, these two extremes correspond to $q \gg 1$ and $q \ll 1$ respectively. It can be shown that the number of stars scattered into the loss cone in one relaxation time scales with q as

$$\mathcal{F} \times t_r \propto [\ln J_c^2/J_{lc}^2]^{-1}, \quad q \ll 1; \quad (34)$$

$$\propto q^{-1} \propto N, \quad q \gg 1 \quad (35)$$

where the $q \propto N^{-1}$ dependence assumes a galaxy with fixed structural properties, i.e. fixed $(M_{\text{gal}}, r_{\text{gal}})$. This decrease in $\dot{M} t_{\text{gal}}$ at small N is visible in the last row of Figure 10; for $N \lesssim 10^8$, i.e. $M_B \gtrsim -13$, the loss cones in these models are essentially full and \dot{M} is independent of the relaxation time.

The N -dependence is illustrated more clearly in Figure 11 which shows \dot{M} and $\int \dot{M} dt$ for the same models, expressed this time in units of solar masses and years; equations (2) and (25) were used to convert N and t_{gal} into physical units. Each of these models evolves in nearly the same way when expressed in terms of t/t_{gal} ; as discussed above, changing the flux of stars into the loss cone has very little effect on the density evolution. The differences in the curves of Figure 11 are due primarily to the different time scaling (small galaxies evolve faster) and secondarily to changes in $q(E)$ as $\rho(r)$ evolves.

The initial disruption rate scales almost linearly with galaxy mass. This dependence is most easily understood in the small- N /full-loss-cone limit, where $\dot{M} \propto M_{\text{gal}}/t_{\text{cr}} \propto (M_{\text{gal}}/t_{\text{rh}})(t_{\text{rh}}/t_{\text{cr}})$ with t_{cr} the galaxy crossing time. From Figure 1a, $t_{\text{rh}} \sim M_{\text{gal}}$, and $t_{\text{rh}}/t_{\text{cr}} \sim N \sim M_{\text{gal}}$, so $\dot{M} \sim M_{\text{gal}} \sim N$. This is similar to the dependence reported in other studies, e.g. Figure 21 of Freitag et al. (2006) who considered black holes in power-law nuclei.

After the Bahcall-Wolf cusp is established, the evolution of \dot{M} is dominated by the systematic decrease in nuclear density. The dashed lines in the top panel of Figure 11, which accurately reproduce the disruption rates for $t \gtrsim t_r(r_{\text{bh}})$, are

$$\dot{M} = 1.8 \times 10^{-7} M_{\odot} \text{ yr}^{-1} \left(\frac{M_{\text{gal}}}{10^8 M_{\odot}} \right) \left(\frac{t}{10^9 \text{ yr}} \right)^{-3/4}. \quad (36)$$

The bottom panel shows time-integrated masses; these are roughly $10^{-2} M_{\text{bh}}$ at $t = 10$ Gyr in all the models.

Tidal destruction rates computed in the past for luminous E galaxies have generally been found to decrease with increasing galaxy/black hole mass (Syer & Ulmer 1999; Magorrian & Tremaine 1999; Wang & Merritt 2004), opposite to the trend shown here in Figure 11. One reason is probably the rather different models used in these studies for representing $\rho(r)$, e.g. “Nuker” models which have unbroken power-law cusps at small radii (Byun et al. 1996). These are reasonable models for some galaxies but do not reproduce the nuclear star clusters of low-luminosity ellipticals (Ferrarese et al. 2006b). Figure 12 plots disruption rates from Wang & Merritt (2004) for a sample of galaxies modelled with Nuker profiles, compared with dN/dt from the Series IV models at four different times: 0.01, 0.1, 1 and 10 Gyr. The rates computed here at $t = 0$ trace the lower envelope of the points from Wang & Merritt (2004).

While these results suggest that tidal disruption rates for some of the galaxies modelled by Wang & Merritt (2004)

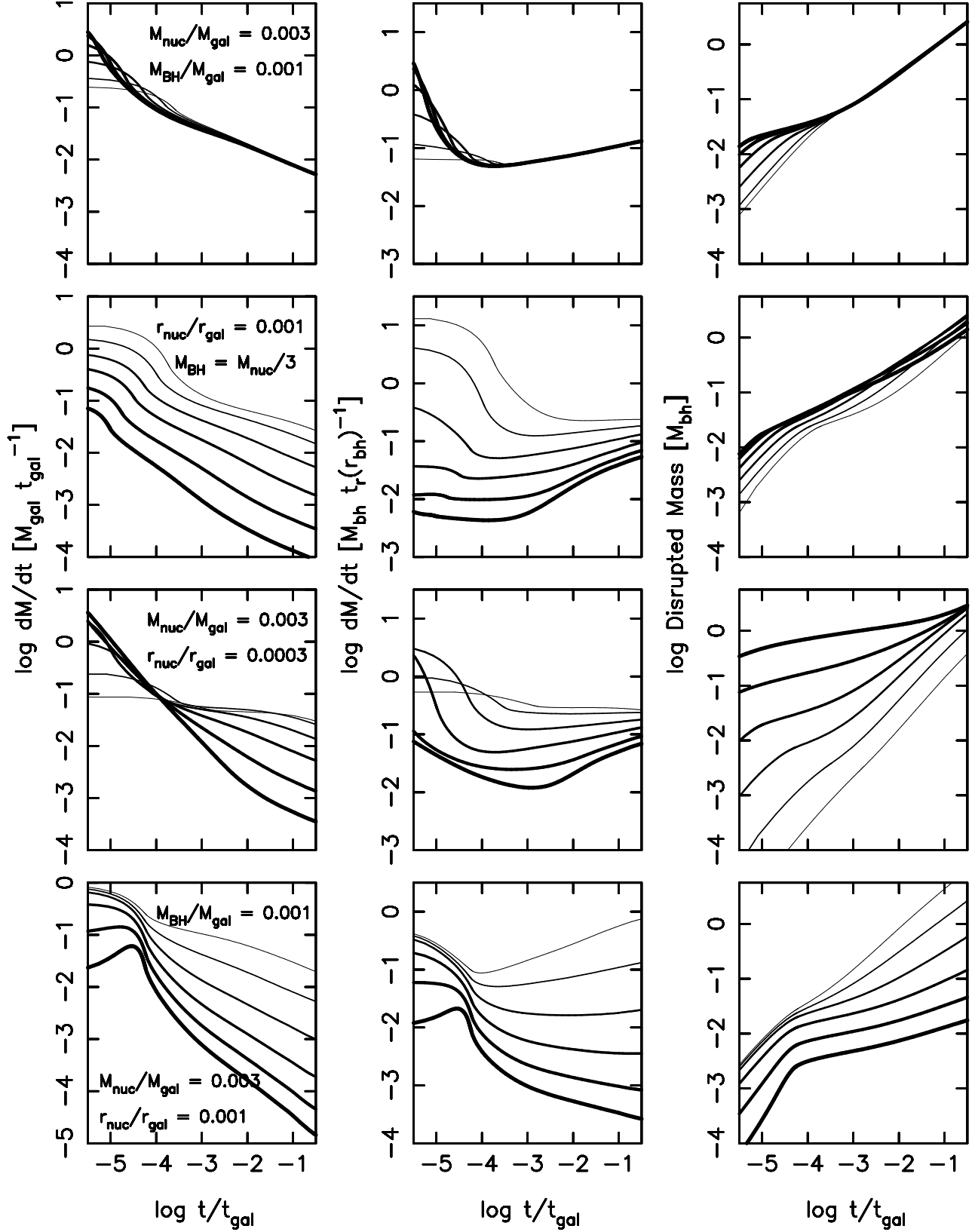


FIG. 10.— *Left column:* Rate at which mass is scattered into the tidal disruption sphere of the black hole, expressed in units of the galaxy mass divided by the galaxy half-mass relaxation time (both of which are constant). *Middle column:* Same as the left column, except that the loss rate is expressed in units of black hole mass divided by the (time-varying) relaxation time at the black hole influence radius r_{bh} . *Right column:* The integral until time t of dM/dt , i.e. the total mass scattered into the black hole's disruption sphere, in units of the (constant) black hole mass. Lines and line widths correspond to the same models in Figures 8 and 9. The bottom panel shows, in addition, models from Series IV, with $\log_{10} N = (6, 7, 8, 9, 10, 11)$; line width decreases with increasing N .

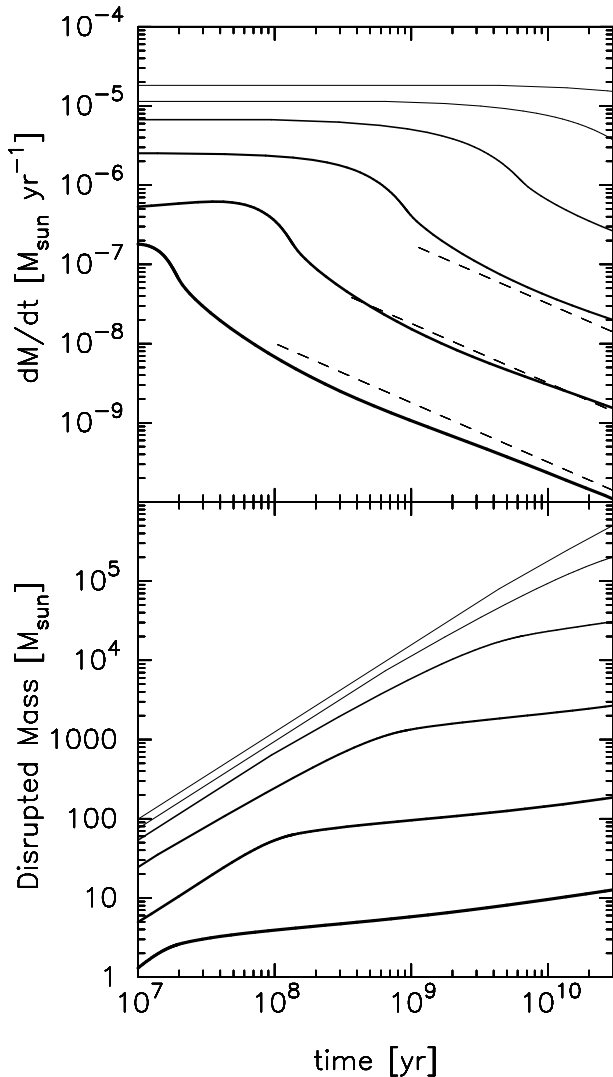


FIG. 11.— *Top*: Stellar tidal disruption rate vs. time for models from Series IV, which have fixed initial structural parameters but which vary in their assumed total mass M_{gal} and hence in the number of stars, $N = M_{\text{gal}}/M_{\odot}$. Curves correspond to N values ranging from 10^6 (thickest) to 10^{11} (thinnest) increasing in steps of 10; the corresponding galaxy luminosities range from $M_B = -8$ to $M_B = -20.5$. Black hole masses are fixed at $10^{-3}M_{\text{gal}}$. Dashed lines are defined in the text (eq. 36). *Bottom*: Total disrupted mass. Galaxy relaxation times have been assumed to scale with galaxy luminosity as in eq. 2.

might have been over-estimated, such a conclusion is probably premature until detailed models can be constructed based on the newest luminosity profiles for these galaxies. Six of the

galaxies in the Wang & Merritt sample are classified as “nucleated” (Type Ia or Type Ib) by Côté et al. (2006). Inspection of the ACS luminosity profiles of these galaxies suggests that none of them exhibit a clear, two-component structure like that of NGC 205; a “Nuker” model might therefore provide an adequate fit to these galaxies.

Figure 12 also emphasizes the strong time dependence of \dot{N} in low-luminosity galaxies, due to the structural changes caused primarily by transfer of heat from the galaxy. This plot suggests that tidal flaring rates in dE galaxies are likely to be a strong function of the time since nuclear formation.

5. SUMMARY

1. Half-mass relaxation times in nuclear star clusters are interestingly short, ranging from ~ 10 Gyr in galaxies with absolute magnitude $M_B = -18$ to ~ 1 Gyr at $M_B = -15$.
2. In the absence of a massive black hole, evolution of nuclear star clusters is a competition between core collapse and heating from the external galaxy. Observed nuclei appear to be in the core-collapse regime, with the exception of nuclei in the brightest galaxies whose relaxation times are so long that they would not evolve appreciably in 10 Gyr.
3. Adding a massive black hole “turns off” core collapse, and nuclear star clusters containing black holes always expand, due primarily to heat input from the galaxy, but also due to the effective heating associated with stellar tidal disruptions. Nuclei with modest black holes dissipate more quickly than black-hole-free nuclei; large black holes, on the other hand, tend to slow the transfer of heat from the galaxy by reducing the temperature gradient.
4. Rates of stellar tidal disruption generally decrease with time due to the drop in density of the nucleus. Rates are lower in galaxies of lower mass, assuming that the relation between black hole mass and bulge mass extends to low galaxy luminosities. A simple expression is presented that reproduces the time dependence of the disruption rate in a restricted class of models.

I thank Dan Batcheldor for assistance with the HST point-spread function used in the analysis of the NGC 205 luminosity profile, Laura Ferrarese and Monica Valluri for additional advice on the modelling of this galaxy, and Milos Milosavljevic and Hagai Perets for useful discussions about the dynamics. Stefanie Komossa also provided useful comments. This work was supported by grants AST-0420920 and AST-0437519 from the NSF, grant NNG04GJ48G from NASA, and grant HST-AR-09519.01-A from STScI.

REFERENCES

- Bahcall, J. N., & Wolf, R. A. 1976, *ApJ*, 209, 214
 Bahcall, J. N., & Wolf, R. A. 1977, *ApJ*, 216, 883
 Baumgardt, H., Makino, J., & Ebisuzaki, T. 2004, *ApJ*, 613, 1133
 Baumgardt, H., Makino, J., Hut, P., McMillan, S., & Portegies Zwart, S. 2003, *ApJ*, 589, L25
 Bekki, K., Couch, W. J., & Shioya, Y. 2006, *ApJ*, 642, L133
 Binggeli, B., Tammann, G. A., & Sandage, A. 1987, *AJ*, 94, 251
 Boeker, T. 2007, to appear in “The impact of HST on European Astronomy” (41st ESLAB Symposium). ArXiv e-prints, 708, arXiv:0708.1093
 Böker, T., Laine, S., van der Marel, R. P., Sarzi, M., Rix, H.-W., Ho, L. C., & Shields, J. C. 2002, *AJ*, 123, 1389
 Böker, T., Sarzi, M., McLaughlin, D. E., van der Marel, R. P., Rix, H.-W., Ho, L. C., & Shields, J. C. 2004, *AJ*, 127, 105
 Byun, Y.-I., et al. 1996, *AJ*, 111, 1889
 Carollo, C. M., Stiavelli, M., de Zeeuw, P. T., & Mack, J. 1997, *AJ*, 114, 2366
 Carollo, C. M., Stiavelli, M., & Mack, J. 1998, *AJ*, 116, 68
 Carollo, C. M., Stiavelli, M., Seigar, M., de Zeeuw, P. T., & Dejonghe, H. 2002, *AJ*, 123, 159
 Carter, D., & Sadler, E. M. 1990, *MNRAS*, 245, 12P
 Ciotti, L. 1991, *A&A*, 249, 99
 Cohn, H. 1980, *ApJ*, 242, 765
 Cohn, H., & Kulsrud, R. M. 1978, *ApJ*, 226, 1087
 Côté, P., et al. 2004, *ApJS*, 153, 223
 Côté, P. et al. 2006, *ApJS*, 165, 57
 De Rijcke, S., Prugniel, P., Simien, F., & Dejonghe, H. 2006, *MNRAS*, 369, 1321

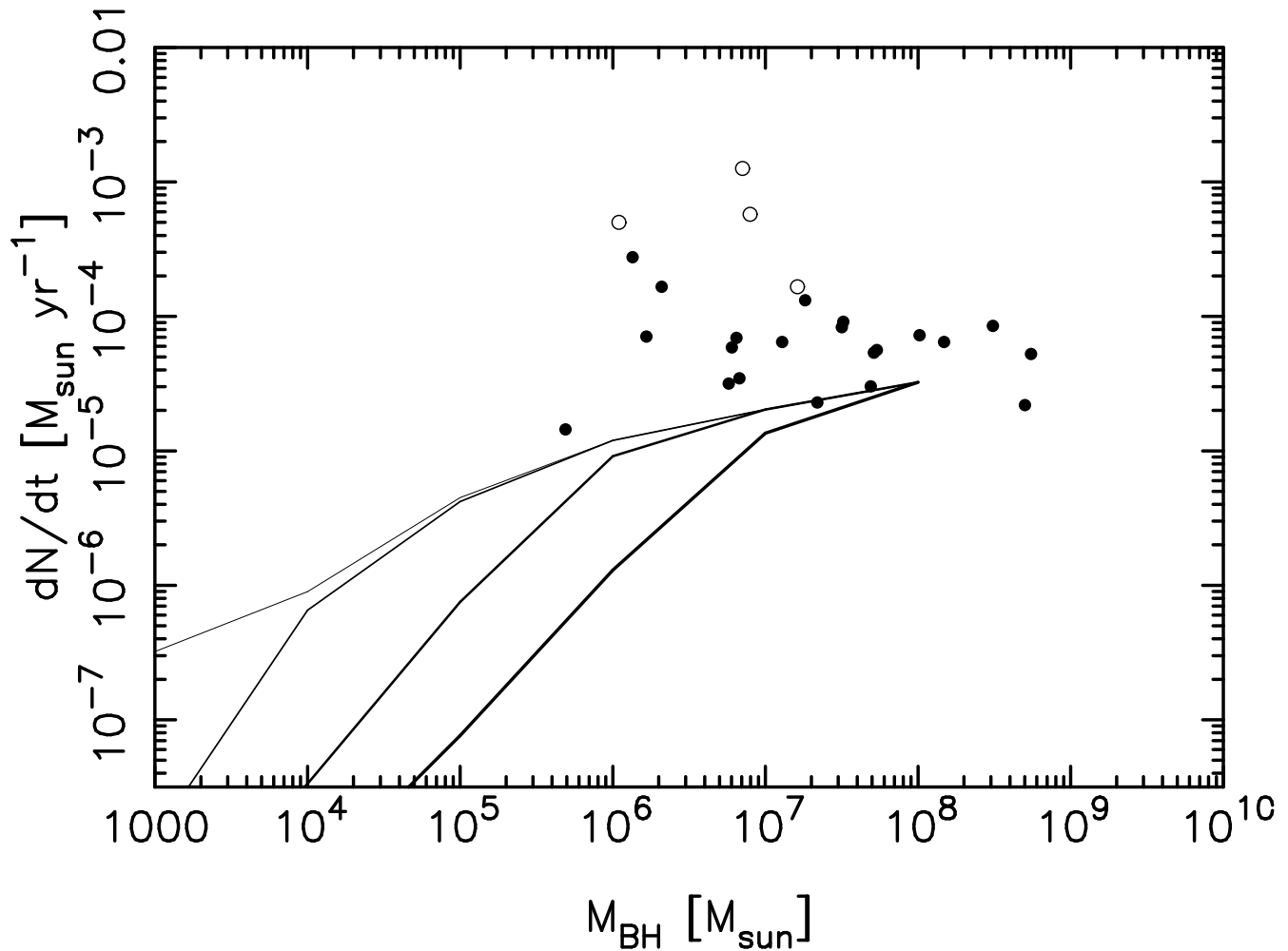


FIG. 12.— Points are stellar tidal disruption rates computed by Wang & Merritt (2004) for a sample of early-type, “power-law” galaxies, with luminosity profiles parametrized as “Nuker” laws. Open circles are galaxies for which the inner (projected) slope parameter Γ of the Nuker-law fit was 0.9 or greater, corresponding to a $\rho \sim r^{-2}$ spatial density profile for the inner parts of the galaxy. Lines show disruption rates in the Fokker-Planck models from Series IV (Fig. 11) at four times, 0.01 Gyr (thin line), 0.1 Gyr, 1 Gyr and 10 Gyr (thick line).

- Decarli, R., Gavazzi, G., Arosio, I., Cortese, L., Boselli, A., Bonfanti, C., & Colpi, M. 2007, astro-ph/0707.0999, 707
- Dokuchaev, V. I., & Ozernoi, L. M. 1985, Soviet Astronomy Letters, 11, 139
- Einasto, J. 1965, Trudy Inst. Astrofiz. Alma-Ata, 5, 87
- Ferrarese, L., Cote, P., Blakeslee, J. P., Mei, S., Merritt, D., & West, M. J. 2006b, In “Black Holes: from Stars to Galaxies - Across the Range of Masses”, proceedings IAU Symposium No. 238, eds. V. Karas & G. Matt. ArXiv Astrophysics e-prints, arXiv:astro-ph/0612139
- Ferrarese, L. et al. 2006a, ApJ, 644, L21
- Ferrarese, L., & Ford, H. 2005, Space Science Reviews, 116, 523
- Filippenko, A. V., & Ho, L. C. 2003, ApJ, 588, L13
- Filippenko, A. V., & Sargent, W. L. W. 1985, ApJS, 57, 503
- . 1989, ApJ, 342, L11
- Freitag, M., Amaro-Seoane, P., & Kalogera, V. 2006, ApJ, 649, 91
- Gonzalez Delgado, R. M., Perez, E., Cid Fernandes, R., & Schmitt, H. 2007, ArXiv e-prints, 710
- Graham, A. W., & Driver, S. P. 2007, ApJ, 655, 77
- Graham, A. W., & Guzmán, R. 2003, AJ, 125, 2936
- Greene, J. E., & Ho, L. C. 2007, ApJ, 667, 131
- Haberl, F., et al. 2000, A&AS, 142, 41
- Ho, L. C. 1999, ApJ, 516, 672
- Hodge, P. W. 1973, ApJ, 182, 671
- Jensen, J. B., Tonry, J. L., Barris, B. J., Thompson, R. I., Liu, M. C., Rieke, M. J., Ajhar, E. A., & Blakeslee, J. P. 2003, ApJ, 583, 712
- Jones, D. H., et al. 1996, ApJ, 466, 742
- Jones, D. H. et al. 2004, MNRAS, 355, 747
- Kim, S. C., & Lee, M. G. 1998, Journal of Korean Astronomical Society, 31, 51
- King, I. R. 1966, AJ, 71, 64
- Komossa, S., & Bade, N. 1999, A&A, 343, 775
- Lee, M. G. 1996, AJ, 112, 1438
- Kandrup, H. E. 1990, ApJ, 364, 100
- Kormendy, J., & McClure, R. D. 1993, AJ, 105, 1793
- Li, Y., Haiman, Z., & Mac Low, M.-M. 2007, ApJ, 663, 61
- Lightman, A. P., & Shapiro, S. L. 1977, ApJ, 211, 244
- Lotz, J. M., Telford, R., Ferguson, H. C., Miller, B. W., Stiavelli, M., & Mack, J. 2001, ApJ, 552, 572
- Maccarone, T. J., Kundu, A., Zepf, S. E., & Rhode, K. L. 2007, Nature, 445, 183
- Magorrian, J., & Tremaine, S. 1999, MNRAS, 309, 447
- Maoz, D., Nagar, N. M., Falcke, H., & Wilson, A. S. 2005, ApJ, 625, 699
- Marconi, A., & Hunt, L. K. 2003, ApJ, 589, L21
- Matthews, L. D. et al. 1999, AJ, 118, 208
- McConnachie, A. W., Irwin, M. J., Ferguson, A. M. N., Ibata, R. A., Lewis, G. F., & Tanvir, N. 2005, MNRAS, 356, 979
- Merritt, D., Navarro, J. F., Ludlow, A., & Jenkins, A. 2005, ApJ, 624, L85
- Merritt, D., Mikkola, S., & Szell, A. 2007, ApJ, 671, 53
- Meylan, G., Sarajedini, A., Jablonka, P., Djorgovski, S. G., Bridges, T., & Rich, R. M. 2001, AJ, 122, 830
- Mickaelian, A. M., et al. 2006, A&A, 449, 425
- Mihos, J. C., & Hernquist, L. 1994, ApJ, 437, L47
- Milosavljević, M. 2004, ApJ, 605, L13
- Milosavljević, M., & Merritt, D. 2001, ApJ, 563, 34
- Moran, E. C., Halpern, J. P., & Helfand, D. J. 1996, ApJS, 106, 341
- Mukai, K. 1993, Legacy, vol. 3, p.21-31, 3, 21
- Nagar, N. M., Falcke, H., & Wilson, A. S. 2005, A&A, 435, 521
- Portegies Zwart, S. F., Baumgardt, H., Hut, P., Makino, J., & McMillan, S. L. W. 2004, Nature, 428, 724

- Ptak, A., & Griffiths, R. 2003, in *Astronomical Society of the Pacific Conference Series*, Vol. 295, *Astronomical Data Analysis Software and Systems XII*, ed. H. E. Payne, R. I. Jedrzejewski, & R. N. Hook, 465–+
- Quinlan, G. D. 1996, *New Astronomy*, 1, 255
- Ravindranath, S., Ho, L. C., Peng, C. Y., Filippenko, A. V., & Sargent, W. L. W. 2001, *AJ*, 122, 653
- Reaves, G. 1977, *PASP*, 89, 620
- Romanishin, W., Strom, K. M., & Strom, S. E. 1977, *BAAS*, 9, 347
- Rossa, J., van der Marel, R. P., Böker, T., Gerssen, J., Ho, L. C., Rix, H.-W., Shields, J. C., & Walcher, C.-J. 2006, *AJ*, 132, 1074
- Sandage, A., Binggeli, B., & Tammann, G. A. 1985, *AJ*, 90, 1759
- Scarlata, C. et al. 2004, *AJ*, 128, 1124
- Schödel, R. et al. 2007, *A&A*, 469, 125
- Sérsic, J. L. 1963, *Boletín de la Asociación Argentina de Astronomía La Plata Argentina*, 6, 41
- Seth, A., Agueros, M., Lee, D., & Basu-Zych, A. 2008, *ApJ*, 678, 116
- Shapiro, S. L. 1977, *ApJ*, 217, 281
- Shields, J., Walcher, C. J. M., Boeker, T., Ho, L. C., Rix, H.-W., & van der Marel, R. P. 2008, *submitted*
- Shields, J. C. et al. 2007, *ApJ*, 654, 125
- Spitzer, L. 1987, *Dynamical Evolution of Globular Clusters* (Princeton: Princeton University Press)
- Syer, D., & Ulmer, A. 1999, *MNRAS*, 306, 35
- Terashima, Y., & Wilson, A. S. 2003, *ApJ*, 583, 145
- Tremaine, S. et al. 2002, *ApJ*, 574, 740
- Trenti, M. 2006, *astro-ph/0612040*
- Valluri, M., Ferrarese, L., Merritt, D., & Joseph, C. L. 2005, *ApJ*, 628, 137
- van den Bergh, S. 1986, *AJ*, 91, 271
- van der Marel, R. P. 2004, in *Coevolution of Black Holes and Galaxies*, ed. L. C. Ho, 37–+
- van der Marel, R. P., Rossa, J., Walcher, C. J., Boeker, T., Ho, L. C., Rix, H.-W., & Shields, J. C. 2007, *IAU Symposium*, 241, 475
- Walcher, C. J., Böker, T., Charlot, S., Ho, L. C., Rix, H.-W., Rossa, J., Shields, J. C., & van der Marel, R. P. 2006, *ApJ*, 649, 692
- Walcher, C. J. et al. 2005, *ApJ*, 618, 237
- Wang, J., & Merritt, D. 2004, *ApJ*, 600, 149
- Wehner, E. H., & Harris, W. E. 2006, *ApJ*, 644, L17